Materials & Design 206 (2021) 109758

Contents lists available at ScienceDirect

Materials & Design

journal homepage: www.elsevier.com/locate/matdes

Biomechanical characterization of custom-made dynamic implants fabricated by Electron Beam Melting for anterior chest wall reconstruction

María Paula Fiorucci [a,*], Alberto Cuadrado [a], Alejandro Yánez [a], Oscar Martel [a], Belinda Mentado [b,c], Donato Monopoli [b,c]

[a] Department of Mechanical Engineering, University of Las Palmas de Gran Canaria, 35017 Las Palmas de Gran Canaria, Spain
[b] Department of Biomedical Engineering, Technological Institute of the Canary Islands (ITC), 35118 Arinaga, Spain
[c] Osteobionix S.L, 35118 Arinaga, Spain

ARTICLE INFO

Article history:
Received 4 November 2020
Revised 24 March 2021
Accepted 20 April 2021
Available online 22 April 2021

Keywords:
Custom-made dynamic implant
Electron Beam Melting
Biomechanical analysis
Ti-6Al-4V
Chest wall reconstruction

ABSTRACT

Large thoracic defects need to be reconstructed to restore inner organs protection and normal ventilation. Early rigid implants have provided the stabilization of the ribcage; however, those have been associated with breathing restrictions. The evolution of additive manufacturing has enabled the production of 3D custom-made thoracic implants. This has led to case reports on reconstructions with these prostheses, particularly for large anterior resections. A novel design of thoracic implant with dynamic capacity has already been reported, with promising short-term outcomes. However, specific biomechanical studies are needed to clarify its mechanical behaviour. A study of the evolution of the design of dynamic thoracic implants was carried out and such implants were biomechanically tested. Furthermore, finite element analyses were carried out to obtain a simple and reliable model to predict the implant behaviour, considering a rib and its costal cartilage. In the models, the stiffness and stress distribution along the implant and the bone showed that the reconstructions exhibited adequate mechanical behaviour. One of the designs provided a flexibility that closely matched the native model and the maximum stress values did not exceed the 30% of the yield strength of Ti-6Al-4V. The implants strength was demonstrated to be sufficient under tested conditions.

1. Introduction

Chest wall defects generally result from resection of primary chest wall tumours, locally-invasive malignancies or metastatic lesions, radiation injury, infection, or trauma [1,2]. The primary goals of chest wall reconstruction include the restoration of the chest wall rigidity (skeletal stability) to protect intrathoracic organs and to preserve the mechanics of breathing [2,3]. In complex cases, large resection may be required, with more than one rib and several anatomical structures, such as cartilages and the sternum, also needed to be removed.

Reconstruction of the chest wall remains controversial regarding the technique to be applied and the type of material or implant to be used [4]. The location and the size of the defect to be reconstructed are principal aspects to take into consideration [3]. Several reconstructive materials have been proposed, including rigid and soft materials, with or without soft tissue covering, such as titanium-based osteosynthesis systems, acrylic or methyl methacrylate resins, cryopreserved allografts, titanium micromesh sandwiched between a layer of polyethylene mesh, or muscular flaps [5].

The progress in the Additive Manufacturing (AM) technology has enabled the production of custom-made implants for chest wall reconstructions. Computed Tomography (CT) data of the patient allow the development of an implant model that completely fulfils the patient's anatomy, based on a precise location and size of the chest wall resection. Demondion et al. [6] fabricated a Ti-6Al-4V sternum which was composed of a plate connected to three staples on each side drawn to be tightened on several ribs. Turna et al. [7] manufactured a single Ti-6Al-4V plate by Selective Laser Melting (SLM) with the shape of the sternum, the clavicles, the first three ribs on the left side and the first four ribs on the right side. Both implants focused mainly on a rigid and static anatomical reconstruction that did not take into account the elongation of the

* Corresponding author at: Edificio de Ingenierías, Campus Universitario de Tafira, 35017 Las Palmas de Gran Canaria, Las Palmas (Canary Islands), Spain.
E-mail address: paula.fiorucci@ulpgc.es (M.P. Fiorucci).

https://doi.org/10.1016/j.matdes.2021.109758
0264-1275/

removed cartilages and the anterior thoracic joints. Another implant design incorporated a rigid sternal core with titanium rods as neo-ribs to improve the flexibility of the implant fabricated by Electron Beam Melting (EBM) in titanium alloy [8].

In recent years, there has been a growing number of publications of case reports on reconstructions with 3D thoracic implants [9–13]. Although rigid methods ensure stabilization of skeletal elements of the chest for breathing balance [14], they are associated with difficulty to anatomical fitting, implant migration, dislocation, infection and failure [2,15]. The lack of implant flexibility would difficult following breathing movements of the thorax and might cause patient discomfort during ventilation. Respiratory complications have been reported as the main source of morbidity after chest wall reconstruction [16,17].

A novel design of custom thoracic implant has been recently originated. The design was adapted to mimic the mechanical behaviour of the tissues to be replaced along with chest reconstruction: an equivalent region of the ribcage formed by cartilage and rib, including the sternocostal joint. A dynamic concept was introduced by a ground-breaking design with a spring-like geometry which makes the implant flexible. The implants have been fabricated by EBM and SLM from Ti-6Al-4V powder and have been clinically tested in singular patients who required large anterior chest wall resection [18–21]. According to some postoperative dynamic studies, the novel design has proven to be able to mimic the behaviour of the natural chest wall during ventilation and to maintain an adequate respiratory function [19,20]. Those previous clinical results give promising evidence that the novel spring-like implant is an optimal choice for reconstructive application in wide anterior chest wall resection. Although clinical reports have described the novel surgical procedure and patient short-term outcomes, more patient cases, long-term clinical follow-up, as well as specific biomechanics studies, are still required.

Overall, the ideal implant should restore the native stiffness of the ribcage and be sufficiently flexible to accommodate breathing. In general, anterior chest wall reconstruction requires variable implantable solutions, including total, partial or no sternum structure associated with one or several cartilage-ribs. To advance safely in the use of customized devices, it is imperative to investigate into a harmless implant design and to clarify the mechanical characteristics that thoracic implants must have.

The main goal of this study is to present the rationale of the design and the biomechanical characterization of a previously reported dynamic thoracic implant in anterior chest wall reconstruction. Based on the presented grounds, in this study it is suggested that the mechanical properties of a 3D printed thoracic implant can be enhanced by optimizing the design of the implant, in terms of flexibility and strength. In the present work, the dynamic implant structures were tested by means of experimental and Finite Element (FE) studies.

2. Materials and methods

2.1. Design and manufacturing of thoracic implants

The original idea of the design made to obtain dynamic implants started with a simple wavy pattern design resembling a spring-like shape device. Hence, the first design approach was based on a wavy shape and was designated as sample *S0* (Fig. 1a). In order to estimate the general mechanical behaviour of *S0*, an arbitrary range of thickness (T) was selected. The thickness range was [1.6; 2; 2.7; 3.4; 4.1] mm and the width (W) was 13 mm.

Based on the results of the preliminary testing (detailed below), new typologies were designed to improve the folding pattern. One of the samples, named *S1*, was designed with variable T and W. The centre of *S1* had T = 2.5 mm and W = 14 mm, continuously growing until reaching ends of T = 2.7 mm and W = 15 mm (Fig. 1b). A third sample was designed (*S2*), introducing a variation in folding form by rolling it up in a longitudinal axis which resulted in a tubular-like shape. *S1* and *S2* had the same T and W gradients towards the extremities (Fig. 1c).

The additive manufacturing of the implants was done by EBM developed by Arcam AB (Krokslätts Fabriker, Mölndal, Sweden) from Ti-6Al-4V-ELI powder (with an average diameter of 50 μm, ARCAM AB). The fabrication procedure was on a stainless-steel start plate and the working parameters were set to generate melting layers of 70 μm. The process was kept under vacuum at 10^{-3} mbar, controlled by Helium. A constant temperature of 700 °C was maintained inside the vacuum chamber throughout the fabrication. Post-processing of the implants was carried out by removing the fabrication supports and mechanical polishing of the surface because of the high roughness of the EBM fabrication [22].

2.2. Experimental tests

Quasi-static three-point bending tests were carried out. A servo-mechanical testing machine was used for bending tests, according to ASTM standards F 382–99 and ISO 9585. A customized semi-circular head was built to adapt the servo actuator to achieve a distributed load on the implants (Fig. 2a). The actuator displacement velocity was 2 mm/min and the load was applied until failure. The 3D implants were fabricated embedded into supports which maintained both ends of the samples fixed (fixed–fixed condition).

The curves of force versus displacement were obtained. The structural stiffness of each specimen was obtained as the slope of the linear part of each force–displacement curve.

2.3. Finite element models

The proposed methodology for the FE analyses is presented in three stages. The FE software used was Abaqus 6.14–2 (Dassault System, SIMULIACorp., Providence, RI, USA).

The first FE analysis was performed on the CAD models of the three designs of the implants (*S0*, *S1* and *S2*) to conduct a biomechanical analysis of the thoracic implants. A replica of experimental three-point bending tests was carried out by FE models. An elastic modulus of 93 GPa and a Poisson's ratio of 0.3 was applied to the elastic model and a yield stress of 869 MPa was applied to the plasticity model [23–25]. To simulate the boundary conditions of the three-point bending tests, the ends of the samples were fixed, and a displacement of 25 mm was applied through the cross-head of the testing machine. This part was considered as having infinite stiffness because it did not affect the computational study. The contact between the cross-head and the samples was a frictionless surface-to-surface interaction (Fig. 2b). After conducting the relevant sensitivity tests, the type of element selected for the mesh was a ten-node tetrahedral element (C3D10). Estimation of stiffness and von Mises stress distribution of the implants were obtained.

The second computational analysis was focused on the development of an anatomical model of the sub-structural level of the ribcage, i.e. a semi rib-ring of the thoracic cage. For that purpose, from the CT scan of a complete thorax obtained from a healthy male subject, the third right rib and its costal cartilage were isolated from the sternum to the spine. Only the right segment of the semi rib-ring was considered for simplification of analysis [26]. All the joints were also removed from the analysis. This model was referred to as "the native model". The STL files from the CT scan were used for the segmentation and reconstruction with the Simpleware commercial package (Synopsys International Ltd., CA, USA). Then, the volumetric meshes were obtained in order to

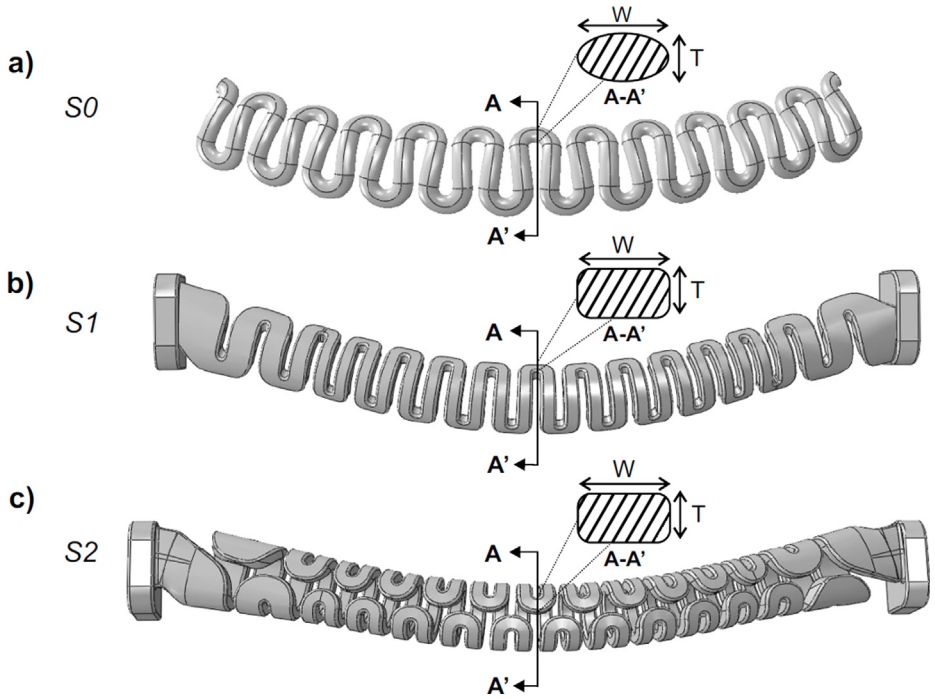

Fig. 1. Designs of the thoracic implants: a) sample S0; b) sample S1; c) sample S2. The cutting plane (A-A') and the cross-sectional area A-A' are represented to indicate the dimensions T and W.

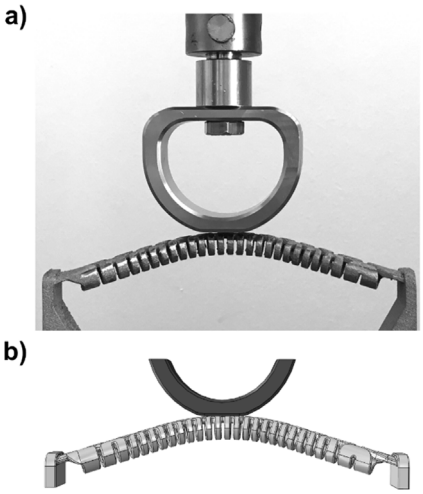

Fig. 2. 3-point bending test. a) Experimental set-up. b) Representation of the contact between the machine head and the sample (S2) in FE simulations.

export to Abaqus. The costal cartilage was modelled as a solid segment with a circular cross-section with a length that allowed the continuity from rib end to sternum along the anatomical circumference.

All tissue behaviours were modelled as isotropic linear elastic materials and material properties were obtained from the literature. The cortical rib bone had Young's modulus (E) and Poison's ratio (v) of 14.4 GPa [27] and 0.3 [28], respectively. The trabecular rib bone had E = 40 MPa and v = 0.35 [28]. The costal cartilage had an E = 35.8 MPa (average value obtained for the third cartilage) and v = 0.40 [29]. The costal cartilage is a composite structure, formed by a central mid-substance of hyaline cartilage surrounded by a fibrous layer, the perichondrium, and those structures exhibited different local material properties which can affect the overall stiffness of the ribcage [29]. Hence, a homogeneous representation of costal cartilage was modelled with an effective E necessary to reproduce the structural behaviour of whole costal cartilage segment [29–31].

A set of loading and boundary conditions were established to analyse the biomechanical response of the semi rib-ring under simulated physiological loads and to predict the overall stiffness of the native model. A simplified loading scenario was reproduced, where the vertebral rib end was articulated and the sternal end was displaced 10 mm towards the posterior end in the plane which best fitted the shape of the cartilage and the rib, to create an anterior-posterior load causing the bending deformation [28]. A single rotational degree of freedom, on an axis normal to the loading plane, was permitted at the posterior extremity. No movement was allowed at the costochondral junction [32]. Estimation of stiffness and stress distribution were carried out. The described model can be observed in Fig. 3a.

The third computational analysis was developed to model the reconstruction of a single right rib with a 3D thoracic implant. In this reconstructed model, the cartilage and an anterior portion of the rib were removed, and the remaining rib portion was reconstructed with *S1* and *S2* implant typologies. The rib reconstructed model was simulated in the same manner that the previous native model. The material properties of the thoracic implants used in this model were the same as in the first FE analysis, whereas the properties of the materials of the rib and the boundary conditions and displacement of this third model were the same as in the second FE analysis (Fig. 3b and 3c). Then, a comparative analysis was performed in terms of overall stiffness and stress distribution along the bone and the implant.

3. Results

3.1. Experimental tests

The experimental results of the three-point bending test of *S0* with several thickness values are summarized in Table 1. Maximum values were obtained from the force–deformation curves of

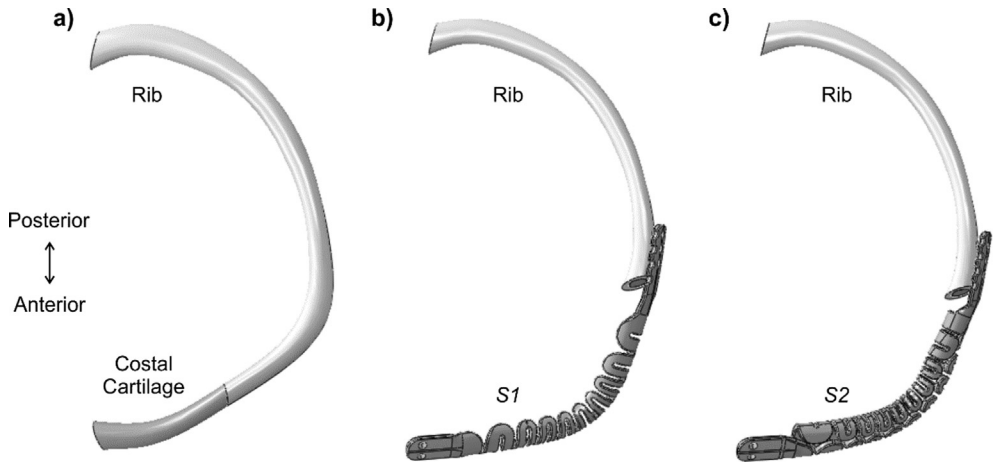

Fig. 3. FE models for a) native condition; b) rib reconstruction with implant S1; and c) rib reconstruction with implant S2.

the loaded implant until failure. The estimation of the stiffness parameter is also given.

There was a relationship, although non-proportional, between the stiffness and the amount of material in the implant. When the sample broke, the failure was at the ends in all samples (Fig. 4a).

Regarding implant *S2*, the experimental results of the three-point bending test showed an average value of peak force and displacement before the failure of (218 ± 41.1) N and (19.6 ± 2.4) mm, respectively, given in mean and standard deviation values. The estimation of the stiffness was (10.1 ± 0.6) N/mm. The failure of the samples was observed to occur in regions located between the centre and the ends (Fig. 4b).

3.2. FE analyses of implant designs

The FE studies were performed first on the CAD design of implant *S0*. When *S0* was loaded, the maximum stresses occurred at the ends of the sample. Fig. 4c depicts the von Mises stress distribution on the *S0* with a thickness of 1.6 mm. A small fraction at the end of the sample was beyond the elastic limit and was coincident with the failure observed in experimental test.

Analogously, the validation of the FE model for implant *S2* was performed based on the results of the previous experimental test presented. Fig. 5 shows the load–displacement curves resulting from both studies. Thus, a good agreement between the experimental and the FE curves was observed.

Once the *S2* FE model was validated, the same set of parameters were implemented into the FE model based on the CAD model of *S1* structure. Then, a comparison between the load–deflection response of the two designed implants was made. Fig. 6 depicts the FE results for the force versus displacement response in the three-point bending test. The estimation of stiffness was obtained from the calculation of the slope of the linear regression, which showed a high goodness of fit index (R^2). The fitting indicated that the implants presented different bending stiffness values: 10.0 N/mm for *S2* and 13.1 N/mm for *S1*.

Von Mises stress distribution for implants *S1* and *S2* were obtained (Fig. 7). The maximum stress values in *S1* were located at the ends of the sample and other critical points at the centre. Only the ends exceeded the yield limit. More homogeneous stress distribution was observed in *S2*. The maximum von Mises stress values were found at smaller points located between the ends and the centre, in consonance with the place where failure was observed (Fig. 4d).

Table 1
Experimental data resulted from the 3-point bending test of the S0 implant with several thickness values.

Sample thickness (mm)	Force (N)	Displacement (mm)	Stiffness (N/mm)
1.6	124	24.19	5.13
2	419	32.89	12.74
2.7	804	29.32	27.42
3.4	811	28.91	28.05
4.1	820	27.56	29.75

3.3. FE analysis of native and reconstructed models

Under the anterior-posterior bending loading simulations in the FE models, a plot of the reaction force at the posterior end of the rib versus deflection applied to the system was obtained for the native model and the reconstruction with implants *S1* and *S2* (Fig. 8). The stiffness of the native model was estimated to be 1.13 N/mm. In the case of reconstruction with implant *S1*, the stiffness was 2.52 N/mm and for implant *S2*, the stiffness was 1.70 N/mm.

The analysis of the stress distribution was performed on the simulated tissues and implants. Fig. 9a depicts the Maximum Principal stress distribution in simulated tissues of the native model. The data are listed in Table 2. The maximum bone stress reached was around 20 MPa in tension (Fig. 9a). An increase in the maximum bone stress value in the range of 22–35 MPa stress was observed when the rib was reconstructed and predominantly occurred at the same location as in the observed for the native model, i.e. on the external convex region of the body of the rib. When comparing the bone stress outcome generated by the rib reconstruction with implant designs, the *S1* reconstruction showed higher maximum bone stress values than the *S2* reconstruction (Table 2, Fig. 9b and c).

In order to clarify the von Mises stress distribution on the implants, cortical and trabecular bones have been hidden in Fig. 10. Different distribution patterns of von Mises stress were exhibited. Implant *S2* showed a more homogeneous stress distribution than *S1*, and the latter also showed higher stress values occurring more frequently. The maximum von Mises stress value for implant *S1* was 328 MPa, whereas for implant *S2* it was 248 MPa (Table 2). Those peak values represented the 40% (implant *S1*) and the 30% (implant *S2*) of the yield stress value of Ti-6Al-4V fabricated by EBM.

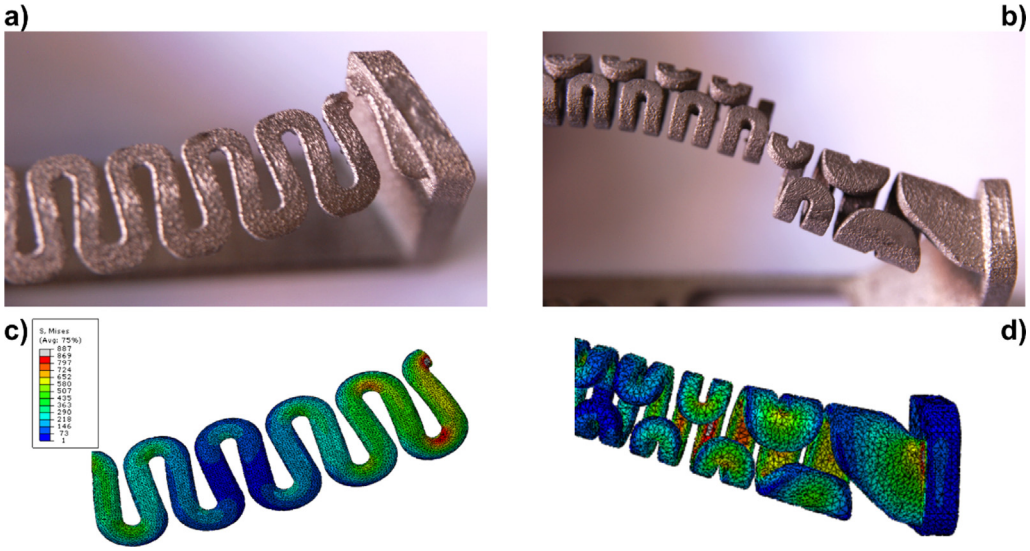

Fig. 4. Examples of the failure of the implants under 3-point bending test. a) S0 sample of 1.6 mm thickness, failure occurred at the ends, b) S2 sample, failure occurred at a region located between the centre and the ends. The von Mises stress distribution in FE simulations revealed the failure prediction for c) S0 and d) S2 samples.

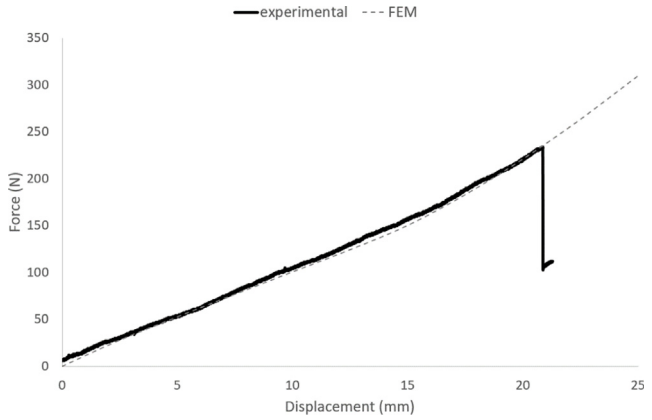

Fig. 5. Force vs displacement response from the 3-point bending test and the results from FE simulation for implant S2.

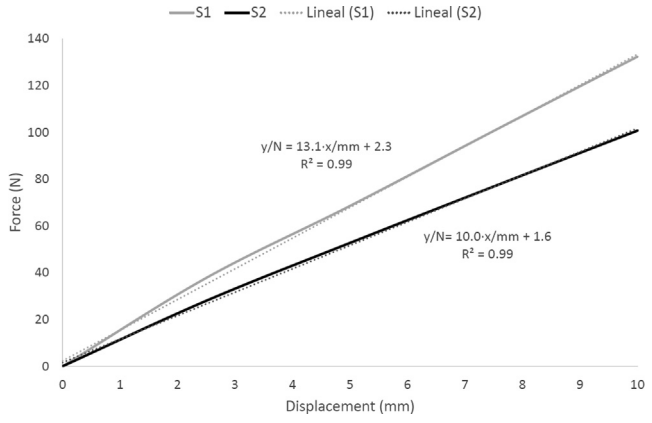

Fig. 6. Force vs displacement responses from FE simulations for implants S2 and S1.

4. Discussion

In this study, the biomechanical characterization of several dynamic designs of custom-made thoracic implants 3D printed by EBM was presented. The goal of the implant designs was to provide a supportive implant able to restore the mechanical integrity of the ribcage, with the strength and the flexibility required by the thorax during a physiological scenario. Implant *S0* was the starting point to develop a dynamic sample. According to FE and experimental results of *S0*, the design was modified in order to obtain a more flexible and stronger structure, thus obtaining implants *S1* and *S2*. The improvements were a greater amount of material at critical points and variations in the implant design. The comparative analyses performed by FE showed that *S2* exhibited more flexibility than *S1*. Consequently, to save supplies and AM machine operating time, the decision was made to fabricate and test only the *S2* samples. Then, the experimental data obtained from the tests were used to validate the FE model to further assess the native and the reconstructed models.

Regarding implant *S0*, the experimental results showed a growing stiffness when increasing the thickness of the design. Furthermore, critical regions prone to failure were observed to be concentrated at both ends of the samples, close to the fixed ends, and this was confirmed by the FE analyses. Those results showed the need to improve the design of the implants to ensure their structural integrity. The extremities of the implant are the anchor points to the healthy bone margin after surgical resection. Hence, improved designs were developed by increasing the amount of material at the ends of the implants (augmented *W* and *T*) and by introducing a variation in the folding of the structure.

The *S1* and *S2* typologies were the new designs made from *S0*. Implant *S1* provided a minor volume due to its low profile. The biomechanical results showed that *S2* provided more flexibility than *S1*. Using a flexible implant would provide an easier and faster anchoring to the anatomical structure during the reconstruction. Its flexibility might also help to absorb potential impacts, preventing it from breakage [18–20]. However, implant *S2* was associated with bulkier shape and with hindering the post-processing after manufacturing (removal of fabrication supports and surface finishing). The von Mises stress analyses showed that the improved designs of *S1* and *S2* (specially *S2)* yielded a more homogeneous stress distribution. Those results suggest that an optimal patient-based design of *S2* typology implant could be able to withstand the stresses generated in the chest wall without breaking.

Several finite element models have been developed to study the human thorax under different physiological or injured scenarios [33–35]. Regarding the biomechanical study of individual compo-

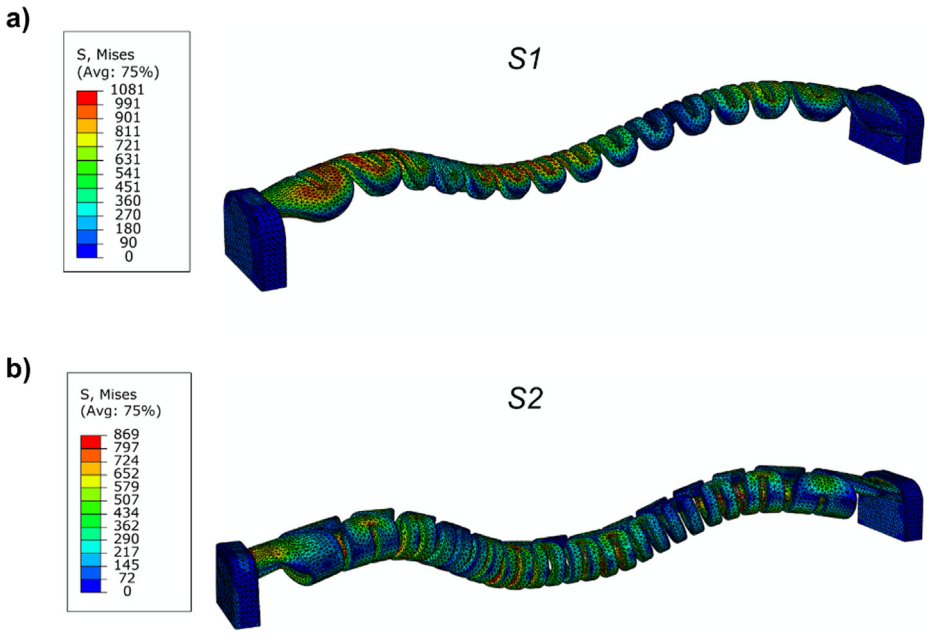

Fig. 7. The von Mises stress distribution of 3-point bending test for implants S1 and S2 under 25 mm of imposed displacement. The machine head was removed from the picture to improve visualization.

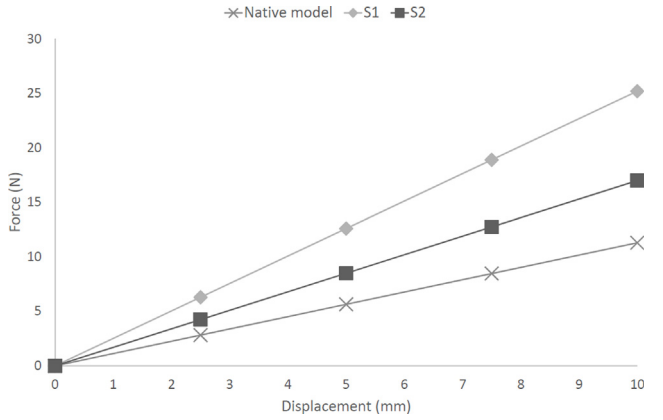

Fig. 8. Force reaction at the posterior end of the rib versus imposed deflection under anterior-posterior loading scenario simulated by FEM for the native and reconstructed models with S1 and S2 implants.

nents of the thorax, several FE models have studied the structural response and fracture prediction of human ribs [28,36,37] and, to a lesser extent, FE models of the costal cartilage [38–40]. However, it was difficult to find FE models that study the biomechanical behaviour of semi rib-ring, formed by an individual rib and its costal cartilage. Such models could give support, on the one hand, to identify the range of mechanical properties ideal for thoracic implant and, on the other hand, to investigate the mechanical coupling of the implant with the rib. Hence, in the present work, the native model of the third right rib and its cartilage developed from CT images of a real patient and the reconstructed model with the proposed implants were studied. The structural stiffness of the native model obtained for the anterior-posterior bending was lower (1.13 N/mm) than values reported for individual ribs in the literature, because the inclusion of the costal cartilage segment in the analysis leads to a decrease in the stiffness of the model. The individual rib stiffness has been reported in the literature [28,41–43]. When the segment of costal cartilage is considered, an accurate model can be assembled, being this model sensitive to *E* variation of the cartilage as it has been reported by other authors [30,38]. An increased range of *E* from 20 to 66 MPa has been reported as a result of high calcification of the cartilage [40]. As it was shown, by changing the design and its parameters, different stiffness values of the implant can be achieved. Particularly, large anterior chest wall reconstruction still represents a challenge to thoracic surgery since a single implant is required to replace ribs, several costal cartilage segments and even the sternum, either partially or completely.

The results of FE simulations of the reconstructed models presented in this study showed that the stiffness of the implant and rib reconstructed mode was slightly higher than that of the native model. Although the estimated stiffness for both models was similar, the reconstruction with *S2* provided the flexibility that matched closer to the native model. A yield stress reference value for cortical bone in the range from 65.3 to 100.7 MPa could be considered [28,33,37]. Despite an increment in the maximum principal stress at the bone with regard to the native model, peak stress values are still far below the referenced strength range, represented by approximately the 42% and 26% of the mean cortical yield stress reference, respectively for implants *S1* and *S2*. The pattern of stress distribution remains still the same on the rib bone. Thus, the reconstruction with the proposed implant would not induce stress concentration that could be harmful or induce further injury at the rib.

Regarding von Mises stress distribution at the implants, the maximum stress reached the 40% for implant *S1* and the 30% for implant *S2* of the yield strength value of Ti-6Al-4V fabricated by EBM. Under the loading scenario and boundary conditions tested, there are no induced maximal stresses that might damage the implant or the rib bone. To date, few studies have focused on the mechanical properties of custom-made thoracic implant manufactured by AM techniques. Due to variations in implant designs, fabrication material, loading condition, etc., comparing results among studies is not always possible. The PEEK rib implant reported by Kang et al. [44] showed that its stiffness was lower than that of

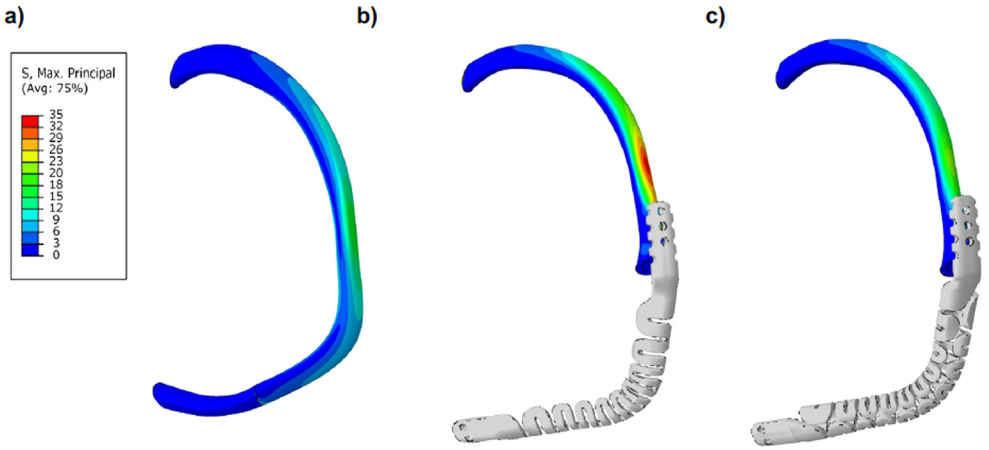

Fig. 9. Maximum principal stress distribution in simulated tissues under anterior-posterior bending in physiological conditions, a) native model, b) rib reconstruction with implant S1, b) rib reconstruction with implant S2. Implants have been painted in grey to indicate that they were removed from the analysis and the mesh has been switched off for improving results interpretation.

Table 2
Stress data of native and reconstructed models under anterior-posterior bending obtained from FE analysis.

Model	max. Principal Stress Bone (MPa)	max. Von Mises Stress Implant (MPa)
Native	18	–
S1 Reconstructed	35	328
S2 Reconstructed	22	248

the modelled natural rib due to the difference of elastic modulus of cortical bone and PEEK material. However, the von Mises stress distribution did not reach critical limits, neither for the implant nor for the rib. Girotti et al. [45] investigated the mechanical behaviour of a ribcage implant made of a polyester mesh and a rigid PMME structure. The numerical response of the complete implant model required about 655 N to displace by about 9 mm, while the bony chest model deflected by 30 mm when about 100 N [45]. The higher stiffness of the implant was attributed to the absence of cartilaginous connections between the ribs and the sternum [45]. The comparison of the results of previous reports with the results presented in this study shows the advantages of the spring-like samples. The dynamic design analysed in the present work has permitted to obtain thoracic implants that can meet the strength requirements with adequate stiffness and to replace a portion of a rib and costal cartilage in a semi rib-ring model. As it was previously reported, dynamic implants have been used to reconstruct thoracic wall with promising clinical results [18–20]. The biomechanical assessment of sample *S2* has contributed to complete the performance description required to move forward in the safe application of these novel custom-made thoracic implants.

The present study exhibits several limitations. *In vivo* rib loading during breathing is a complex mechanism. The current experimental tests and proposed FE models were sought to simplify the loading of a single rib and costal cartilage in very restricted boundary conditions to allow performing replicable testing. Only a selected range of material properties have been tested. There exists a great variability among patient subjects related to the anatomy, as well as the variability of the properties of simulated materials and biological tissues.

Further investigations are needed to test the biomechanical performance of the implant in more demanding scenarios such as coughing, accidental hit/punch or cardiopulmonary resuscitation. Moreover, due to the cycling nature of breathing, it would be essential to perform fatigue analyses of custom-made implants. Even so, the fact that the maximum stress in implant *S2* did not exceed the threshold of 30% of the yield strength value of Ti-6Al-4V fabricated by EBM constitutes a promising result. Additional investigation to

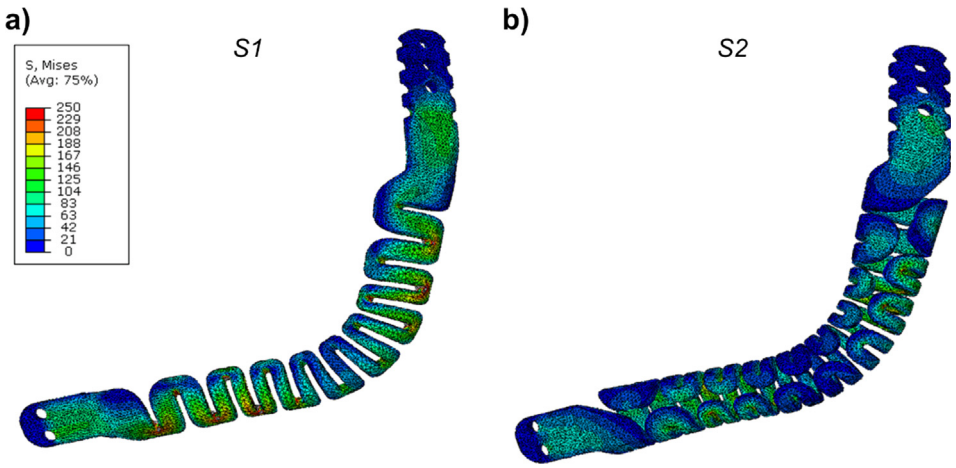

Fig. 10. Von Mises stress distribution on Ti-6Al-4V implants of reconstructed models under antero-posterior bending in physiological conditions. a) implant S1; b) implant S2.

extrapolate the results obtained from the present study to a more realistic model considering the whole ribcage would be highly valuable. In this manner, FE analyses could be integrated in the procedure of a custom-made thoracic implant intervention/surgery, allowing to simulate in the most realistic way the clinical case of the patient before the reconstruction surgery, as a complementary stage in the preoperative planning process.

5. Conclusion

The evolution of the design of thoracic implants carried out in this study demonstrated that through AM fabrication, it is possible to obtain a safe custom-made implant which owns adequate mechanical properties to reconstruct chest wall resections. The design of the special folding pattern in *S2* exhibited the most suitable stiffness since this closely matched the native model. Adjusting parameters of the design could lead to a fine tuning of the biomechanical properties of the implants. The reconstructed model verified that the stress distribution in the rib was not noticeably altered and that the implant strength was sufficient under the tested conditions.

Declaration of Competing Interest

The authors declare that they have no known competing financial interests or personal relationships that could have appeared to influence the work reported in this paper.

Acknowledgement

The authors also acknowledge the Postdoctoral Program grant provided by the University of Las Palmas de Gran Canaria, Spain.

References

[1] C. Deschamps, B.M. Tirnaksiz, R. Darbandi, V.F. Trastek, M.S. Allen, D.L. Miller, P.G. Arnold, P.C. Pairolero, E.A. Rendina, G.A. Patterson, M.K. Ferguson, Early and long-term results of prosthetic chest wall reconstruction, J. Thorac. Cardiovasc. Surg. (1999), https://doi.org/10.1016/S0022-5223(99)70339-9.
[2] C.W. Seder, G. Rocco, Chest wall reconstruction after extended resection, J. Thorac. Dis. 8 (S11) (2016) S863–S871, https://doi.org/10.21037/jtd10.21037/jtd.2016.11.07.
[3] K.A. Mansour, V.H. Thourani, A. Losken, J.G. Reeves, J.I. Miller, G.W. Carlson, G. E. Jones, Chest wall resections and reconstruction: a 25-year experience, Ann. Thorac. Surg. 73 (6) (2002) 1720–1726, https://doi.org/10.1016/S0003-4975(02)03527-0.
[4] P. Ferraro, S. Cugno, M. Liberman, M.A. Danino, P.G. Harris, Principles of chest wall resection and reconstruction, Thorac. Surg. Clin. 20 (4) (2010) 465–473, https://doi.org/10.1016/j.thorsurg.2010.07.008.
[5] K. Harati, J. Kolbenschlag, B. Behr, O. Goertz, T. Hirsch, N. Kapalschinski, A. Ring, M. Lehnhardt, A. Daigeler, Thoracic wall reconstruction after tumor resection, Front. Oncol. (2015), https://doi.org/10.3389/fonc.2015.00247.
[6] P. Demondion, O. Mercier, F. Kolb, E. Fadel, Sternal replacement with a custom-made titanium plate after resection of a solitary breast cancer metastasis, Interact. Cardiovasc. Thorac. Surg. 18 (1) (2014) 145–147, https://doi.org/10.1093/icvts/ivt456.
[7] A. Turna, K. Kavakli, E. Sapmaz, H. Arslan, H. Caylak, H.S. Gokce, A. Demirkaya, Reconstruction with a patient-specific titanium implant after a wide anterior chest wall resection, Interact. Cardiovasc. Thorac. Surg. 18 (2) (2014) 234–236, https://doi.org/10.1093/icvts/ivt408.
[8] J.L. Aranda, M.F. Jiménez, M. Rodríguez, G. Varela, Tridimensional titanium-printed custom-made prosthesis for sternocostal reconstruction, Eur. J. Cardio-Thoracic Surg. 48 (4) (2015) e92–e94, https://doi.org/10.1093/ejcts/ezv265.
[9] J.L. Aranda, N. Novoa, M.F. Jiménez, Thoracic customized modular titanium-printed prosthesis, AME Case Reports (2019) doi:10.21037/acr.2019.08.01.
[10] X. Wen, S. Gao, J. Feng, S. Li, R. Gao, G. Zhang, Chest-wall reconstruction with a customized titanium-alloy prosthesis fabricated by 3D printing and rapid prototyping, J. Cardiothorac. Surg. 13 (2018) 1–7, https://doi.org/10.1186/s13019-017-0692-3.
[11] M.D. Tran, J.A. Varzaly, J.C.Y. Chan, Y. Caplash, M.G. Worthington, Novel Sternal reconstruction with custom three-dimensional–printed titanium porestar prosthesis, Innov. Technol. Tech. Cardiothorac. Vasc. Surg. 13 (4) (2018) 309–311, https://doi.org/10.1097/IMI.0000000000000511.
[12] A. Dzian, J. Živčák, R. Penciak, R. Hudák, Implantation of a 3D-printed titanium sternum in a patient with a sternal tumor, World J. Surg. Oncol. 16 (1) (2018), https://doi.org/10.1186/s12957-018-1315-8.
[13] M.K. Kamel, A. Cheng, B. Vaughan, B. Stiles, N. Altorki, J.A. Spector, J.L. Port, Sternal reconstruction using customized 3D-printed titanium implants, Ann. Thorac. Surg. 109 (6) (2020) e411–e414, https://doi.org/10.1016/j.athoracsur.2019.09.087.
[14] A. Bille, L. Okiror, W. Karenovics, T. Routledge, Experience with titanium devices for rib fixation and coverage of chest wall defects, Interact. Cardiovasc. Thorac. Surg. 15 (4) (2012) 588–595, https://doi.org/10.1093/icvts/ivs327.
[15] P.K. Sharma, T.P. Willems, D.J. Touw, W. Woudstra, M.E. Erasmus, T. Ebels, Implant failure: STRATOS system for pectus repair, Ann. Thorac. Surg. 103 (5) (2017) 1536–1543, https://doi.org/10.1016/j.athoracsur.2016.08.033.
[16] M.J. Weyant, M.S. Bains, E. Venkatraman, R.J. Downey, B.J. Park, R.M. Flores, N. Rizk, V.W. Rusch, Results of chest wall resection and reconstruction with and without rigid prosthesis, Ann. Thorac. Surg. 81 (1) (2006) 279–285, https://doi.org/10.1016/j.athoracsur.2005.07.001.
[17] J.P. Corkum, P.B. Garvey, D.P. Baumann, J. Abraham, J. Liu, W. Hofstetter, C.E. Butler, M.W. Clemens, Reconstruction of massive chest wall defects: A 20-year experience, J. Plast. Reconstr. Aesthetic Surg. 73 (6) (2020) 1091–1098, https://doi.org/10.1016/j.bjps.2020.02.010.
[18] J. Aragón, I. Pérez Méndez, Dynamic 3D printed titanium copy prosthesis: A novel design for large chest wall resection and reconstruction, J. Thorac. Dis. 8 (6) (2016) E385–E389, https://doi.org/10.21037/jtd10.21037/jtd.2016.03.94.
[19] J. Moradiellos, S. Amor, M. Córdoba, G. Rocco, M. Vidal, A. Varela, Functional chest wall reconstruction with a biomechanical three-dimensionally printed implant, Ann. Thorac. Surg. 103 (4) (2017) e389–e391, https://doi.org/10.1016/j.athoracsur.2016.11.048.
[20] J.R. Cano, F.H. Escobar, D.P. Alonso, L.L. Rivero, Reconstruction of the anterior chest wall with a 3-dimensionally printed biodynamic prosthesis, J. Thorac. Cardiovasc. Surg. 155 (1) (2018) e59–e60, https://doi.org/10.1016/j.jtcvs.2017.08.118.
[21] J. Vannucci, E. Scarnecchia, R. Potenza, S. Ceccarelli, D. Monopoli, F. Puma, Dynamic titanium prosthesis based on 3D-printed replica for chest wall resection and reconstruction, Transl. Lung Cancer Res. 9 (5) (2020) 2027–2032, https://doi.org/10.21037/tlcr10.21037/tlcr-20-699.
[22] A. Pérez-Sánchez, A. Yánez, A. Cuadrado, O. Martel, N. Nuño, Fatigue behaviour and equivalent diameter of single Ti-6Al-4V struts fabricated by Electron Bean Melting orientated to porous lattice structures, Mater. Des. 155 (2018) 106–115, https://doi.org/10.1016/j.matdes.2018.05.066.
[23] H.K. Rafi, N. V Karthik, H. Gong, T.L. Starr, B.E. Stucker, Microstructures and Mechanical Properties of Ti6Al4V Parts Fabricated by Selective Laser Melting and Electron Beam Melting, 22 (2013) 3872–3883. doi:10.1007/s11665-013-0658-0.
[24] A. Cuadrado, A. Yánez, O. Martel, S. Deviaene, D. Monopoli, Influence of load orientation and of types of loads on the mechanical properties of porous Ti6Al4V biomaterials, Mater. Des. 135 (2017) 309–318, https://doi.org/10.1016/j.matdes.2017.09.045.
[25] A. Yánez, M.P. Fiorucci, A. Cuadrado, O. Martel, D. Monopoli, Surface roughness effects on the fatigue behaviour of gyroid cellular structures obtained by additive manufacturing, Int. J. Fatigue. 138 (2020) 105702, https://doi.org/10.1016/j.ijfatigue.2020.105702.
[26] N. Yoganandan, F.A. Pintar, Biomechanics of human thoracic ribs, J. Biomech. Eng. 120 (1998) 100–104, https://doi.org/10.1115/1.2834288.
[27] A.R. Kemper, C. McNally, C.A. Pullins, L.J. Freeman, S.M. Duma, S.M. Rouhana, The biomechanics of human ribs: material and structural properties from dynamic tension and bending tests, Stapp Car Crash J. 51 (2007) 235–273.
[28] Z. Li, M.W. Kindig, J.R. Kerrigan, C.D. Untaroiu, D. Subit, J.R. Crandall, R.W. Kent, Rib fractures under anterior-posterior dynamic loads: Experimental and finite-element study, J. Biomech. 43 (2) (2010) 228–234, https://doi.org/10.1016/j.jbiomech.2009.08.040.
[29] J.L. Forman, E. Del Pozo de Dios, R.W. Kent, A pseudo-elastic effective material property representation of the costal cartilage for use in finite element models of the whole human body, Traffic Inj. Prev. 11 (2010) 613–622. doi:10.1080/15389588.2010.517254.
[30] D. Murakami, S. Kobayashi, T. Torigaki, R. Kent, Finite element analysis of hard and soft tissue contributions to thoracic response: sensitivity analysis of fluctuations in boundary conditions., Stapp Car Crash J. 50 (2006) 169–189. https://www.scopus.com/inward/record.uri?eid=2-s2.0-33947507878&partnerID=40&md5=fc5e63cdf168e8c5281c3f2ba6196240.
[31] A. Lau, M.L. Oyen, R.W. Kent, D. Murakami, T. Torigaki, Indentation stiffness of aging human costal cartilage, Acta Biomater. 4 (1) (2008) 97–103, https://doi.org/10.1016/j.actbio.2007.06.008.
[32] S. (Editor-in-C. Standring, ed., Gray's Anatomy: The Anatomical Basis of Clinical Practice, Elsevier Churchill Livingstone, 2005.
[33] H. Kimpara, M. Iwamoto, I. Watanabe, K. Miki, J.B. Lee, K.H. Yang, A.I. King, Effect of assumed stiffness and mass density on the impact response of the human chest using a three-dimensional FE model of the human body, J. Biomech. Eng. 128 (2006) 772–776, https://doi.org/10.1115/1.2264394.
[34] D. Poulard, R.W. Kent, M. Kindig, Z. Li, D. Subit, Thoracic response targets for a computational model: a hierarchical approach to assess the biofidelity of a 50th-percentile occupant male finite element model, J. Mech. Behav. Biomed. Mater. 45 (2015) 45–64, https://doi.org/10.1016/j.jmbbm.2015.01.017.
[35] G. Zhang, X. Chen, J. Ohgi, T. Miura, A. Nakamoto, C. Matsumura, S. Sugiura, T. Hisada, Biomechanical simulation of thorax deformation using finite element approach, Biomed. Eng. Online. 15 (2016) 15–18, https://doi.org/10.1186/s12938-016-0132-y.

[36] Z. Li, M.W. Kindig, D. Subit, R.W. Kent, Influence of mesh density, cortical thickness and material properties on human rib fracture prediction, Med. Eng. Phys. 32 (9) (2010) 998–1008, https://doi.org/10.1016/j.medengphy.2010.06.015.
[37] J. Iraeus, K. Brolin, B. Pipkorn, Generic finite element models of human ribs, developed and validated for stiffness and strain prediction – To be used in rib fracture risk evaluation for the human population in vehicle crashes, J. Mech. Behav. Biomed. Mater. 106 (2020) 103742, https://doi.org/10.1016/j.jmbbm.2020.103742.
[38] A. Vaziri, H. Nayeb-Hashemi, B. Akhavan-Tafti, Computational model of rib movement and its application in studying the effects of age-related thoracic cage calcification on respiratory system, Comput. Methods Biomech. Biomed. Engin. 13 (2) (2010) 257–264, https://doi.org/10.1080/10255840903170694.
[39] J.L. Forman, R.W. Kent, Modeling costal cartilage using local material properties with consideration for gross heterogeneities, J. Biomech. 44 (5) (2011) 910–916, https://doi.org/10.1016/j.jbiomech.2010.11.034.
[40] A.G. Lau, M.W. Kindig, R.S. Salzar, R.W. Kent, Micromechanical modeling of calcifying human costal cartilage using the generalized method of cells, Acta Biomater. 18 (2015) 226–235, https://doi.org/10.1016/J.ACTBIO.2015.02.012.
[41] E. Charpail, X. Trosseille, P. Petit, S. Laporte, F. Lavaste, G. Vallancien, Characterization of PMHS Ribs: A New Test Methodology, in: SAE Tech. Pap., SAE International, 2005, pp. 183–198. doi:10.4271/2005-22-0009.
[42] M. Kindig, A.G. Lau, R.W. Kent, Biomechanical response of ribs under quasistatic frontal loading, Traffic Inj. Prev. 12 (2011) 377–387, https://doi.org/10.1080/15389588.2011.583960.
[43] M.M. Murach, Y.-S. Kang, S.D. Goldman, M.A. Schafman, S.H. Schlecht, K. Moorhouse, I. V Bolte J.H., A.M. Agnew, Rib geometry explains variation in dynamic structural response: potential implications for frontal impact fracture risk, Ann. Biomed. Eng. 45 (2017) 2159–2173. doi:10.1007/s10439-017-1850-4.
[44] J. Kang, L. Wang, C. Yang, L. Wang, C. Yi, J. He, D. Li, Custom design and biomechanical analysis of 3D-printed PEEK rib prostheses, Biomech. Model. Mechanobiol. 17 (2018) 1083–1092, https://doi.org/10.1007/s10237-018-1015-x.
[45] A. Girotti, F. Rosa, M. Ferrotto, P. Girotti, U. Pastorino, Mechanical behavior of a total chest wall prosthesis with rib-like features, Comput. Methods Biomech. Biomed. Engin. 20 (2017) 1581–1588, https://doi.org/10.1080/10255842.2017.1391952.